Journal of Materials Chemistry B

Intracellular Delivery of Virus-Like Particles Using a Sheddable Linker

Journal:	*Journal of Materials Chemistry B*
Manuscript ID	TB-ART-03-2023-000696.R1
Article Type:	Paper
Date Submitted by the Author:	21-Jun-2023
Complete List of Authors:	Hagge, Laurel; The University of Texas at Dallas, Chemistry Shahrivarkevishahi, Arezoo; University of Texas at Dallas Al-Kharji, Noora; The University of Texas at Dallas Chen, Zhuo; The University of Texas at Dallas Brohlin, Olivia R.; The University of Texas at Dallas Ikeda, Trashi; The University of Texas at Dallas, Tumac, Alisia; The University of Texas at Dallas Castro, Fabian; The University of Texas at Dallas Adlooru, Abhinay; The University of Texas at Dallas Lee, Hamilton; The University of Texas at Dallas Firouzi, Hamid; University of Texas at Dallas Cornelius, Samuel; The University of Texas at Dallas Nisco, Nicole J. De; The University of Texas at Dallas Gassensmith, Jeremiah; University of Texas at Dallas, Chemistry and Biochemistry

SCHOLARONE™
Manuscripts

ARTICLE

Intracellular Delivery of Virus-Like Particles Using a Sheddable Linker

Laurel Hagge,[a†] Arezoo Shahrivarkevishahi,[a†] Noora M. Al-Kharji,[a†] Zhuo Chen,[a] Olivia Brohlin,[a] Ikeda Trashi,[a] Alisia Tumac,[a] Fabian C. Herbert,[a] Abhinay Varma Adlooru,[a] Hamilton Lee,[a] Hamid Reza Firouzi,[a] Samuel A. Cornelius,[b] Nicole J. De Nisco,[b] Jeremiah J. Gassensmith [a,c†]

Intracellular targeting is essential for the efficient delivery of drugs and nanotherapeutics. Transporting nanomaterials into cells' cytoplasm for therapeutic purposes can be challenging due to the endosomal trap and lysosomal degradation of cargo. To overcome this issue, we utilized chemical synthesis to design a functional carrier that can escape the endosome and deliver biological materials into the cytoplasm. We synthesized a thiol-sensitive maleimide linker that connects the well-known mitochondria targeting lipophilic triphenylphosphonium cation (TPP) to the surface of a proteaceous nanoparticle based on the engineered virus-like particle (VLP) Qβ. TPP facilitates endosomal escape by its lipophilic and cationic nature, which disrupts the endosomal membrane. Once in the cytosol, glutathione reacts with the thiol-sensitive maleimide linkers, severs the TPP from the nanoparticle, halting its trafficking to the mitochondria, and marooning it in the cytosol. We successfully demonstrated cytosolic delivery of a VLP loaded with Green Fluorescent Protein (GFP) *in vitro* and small-ultrared fluorescent protein (smURFP) *in vivo*, where evenly distributed fluorescence is observed in A549 human lung adenocarcinoma cells and the epithelial cells of BALB/c mice lungs. As a proof of concept, we encapsulated luciferase-targeted siRNA (siLuc) inside the VLP decorated with the maleimide-TPP (M-TPP) linker. We observed enhanced luminescence silencing in luciferase-expressing HeLa cells using our sheddable TPP linker compared to control VLPs.

Introduction

In order for medicine to be effective in diagnosing and treating diseases, such as cancer, genetic disorders, Alzheimer's, and Parkinson's, access to the cell cytoplasm is crucial. [1-4] Cytosolic delivery of nanomaterials and biomacromolecules is fraught with biological barriers—the largest being endosomal escape.[5] There are few entry routes for large or charged macromolecules aside from endocytosis. Once inside the cell endosome, the most likely outcome is eventual lysosomal degradation resulting in a low delivery dose, poor bioavailability, and limited therapeutic efficiency. This limitation has presented itself as a significant challenge, specifically in the cytosolic delivery of large and charged therapeutic cargos and targeted delivery of drugs into the intracellular compartment. Therefore, a delivery system capable of escaping the endosome before lysosomal degradation is needed. Some available delivery systems, including hydrogels,[6] lipid nanoparticles,[7] cell-penetrating peptides,[8] DNA-binding protein nanocages,[9] and metal-organic frameworks,[10,11] have shown potential in promoting cellular uptake, protecting cargo from enzymatic hydrolysis, and enhancing site-specific delivery. However, these systems suffer from various limitations, including leakage of encapsulated cargo, toxicity, and

inefficient delivery that results in low bioavailability. Using chemistry to address biological needs has facilitated advances in research areas such as drug discovery, bioconjugations, and materials science to improve biotherapeutic modalities.[12] This work uses synthetic strategies and methodologies to design a functional carrier that helps biological materials escape the endosome and reach the cell's cytosol. For this purpose, we combined maleimide (M) and triphenylphosphonium (TPP) chemistries to create this function.

The small lipophilic cationic molecule, TPP, has been long exploited as a mitochondrial targeting moiety for small and medium-sized molecules.[13, 14] Cargo tagged with a TPP moiety can escape the endosome and preferentially bind to the negatively charged mitochondrial matrix.[15-17] We wondered if we could promote endosomal escape yet avoid mitochondrial targeting by installing a linker between the nanoparticle and the TPP moiety that degrades once the nanoparticle enters the cytoplasm. TPP is an easily synthesized small molecule with low toxicity and can be chemically functionalized to a wide range of nanoparticle platforms. This gives our approach a distinct advantage over peptides, which are more costly, more complicated to attach to surfaces, and susceptible to enzymatic degradation.

We employed a proteinaceous nanoparticle called a virus-like particle (VLP) to demonstrate our approach. VLPs have emerged as a promising platform for various therapeutic applications ranging from imaging, gene delivery, and drug delivery.[18-22] They are non-infectious, biocompatible, biodegradable, monodisperse, and robust platforms that can carry small molecules,[23, 24] polymers,[25] gold nanoparticles,[26, 27] and/or intact proteins either by supramolecular entrapment within their interior or by chemical conjugation to their surface.[28, 29] The bacteriophage Qβ is a 28 nm icosahedral engineered VLP with 180 identical coat proteins (CPs) that self-assembles around

a. *Department of Chemistry and Biochemistry, , The University of Texas at Dallas, Richardson, Texas 75080, United States*

b. *Department of Biological Sciences, The University of Texas at Dallas, Richardson, Texas 75080, United States*

c. *Department of Bioengineering, The University of Texas at Dallas, Richardson, Texas 75080, United States*

† These authors contributed equally to the article.

random mRNA during expression in E. coli.[30-33] We, and others, have shown that the CPs of Qβ can be disassembled, the random mRNA discarded, and then reassembled around new cargo or genetic material.[31, 33, 34] Furthermore, Qβ possesses functionalizable primary amine groups on three surface-exposed lysine residues (K2, K13, and K16) and the N-terminus (Scheme 1) as well as 180 solvent-exposed disulfide groups that crosslink either six or five proteins to form hexameric (Scheme 1A) and pentameric subunits, respectively. These disulfides can be reduced (Scheme 1B), and the free sulfhydryl groups are effectively "rebridged" in quantitative yields using a maleimide crosslinker (Scheme 1C).[23, 35]

Scheme 1. Structure of Qβ VLP (exposed lysines are labeled in blue, and cysteines are labeled in yellow). Hexameric and pentameric structures are colored green and orange, respectively. A) Close-up of one of the hexameric disulfide-lined pores. B) The disulfides can be reduced quantitatively to produce free sulfhydryl groups. C) These can be crosslinked using a dibromomaleimide reagent. D) The maleimide crosslinkers come off in the presence of glutathione to produce 12 free thiols.
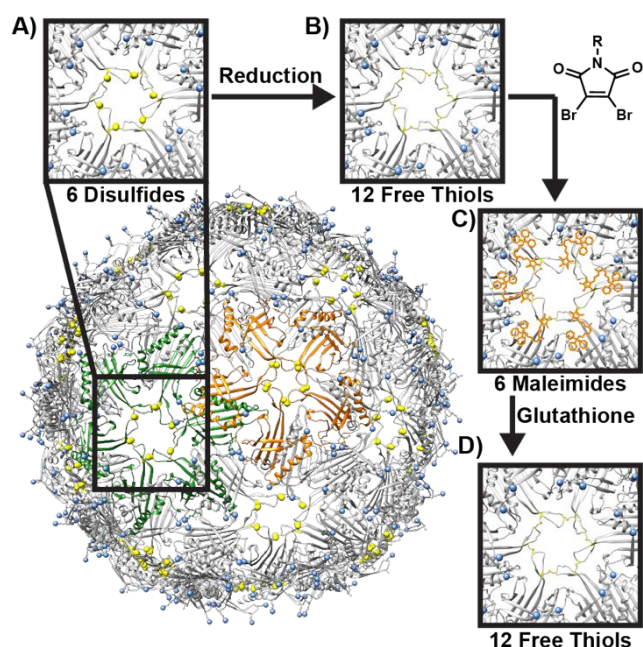
This work demonstrates a "sheddable" cytosolic delivery approach by attaching a TPP-containing moiety through a disulfide-bridging maleimide that forms a stable two-carbon bridge between the sulfurs. The maleimide on the VLP readily undergoes retro-Michael additions in the presence of glutathione (Scheme 1D), which is present in millimolar concentrations (10^{-3} M) in the cytosol but micromolar concentrations (10^{-6} M) outside the cell.[36, 37] In vitro, the TPP-functionalized virus undergoes endocytosis, escapes the endosome, and then sheds the TPP-functionalized maleimide linker through a thiol exchange with glutathione in the cytosol. Moreover, we have developed a single-pot approach that allows us to simultaneously reassemble the virus around genetic cargo with a functionalized dibromomaleimide serving to 'sew up' the capsid.[35] Finally, as proof of principle, we demonstrate the cytosolic delivery of Qβ loaded with GFP in vivo and, in a second example, the in vitro cytosolic delivery of siRNA that stops luciferase expression.

Experimental

Synthesis and characterization of Qβ-M-TPP

TPP has a delocalized positive charge over large hydrophobic phenyl rings, which is known to permeate lipid bilayers and cross into the mitochondrial matrix through non-carrier-mediated transport because of the significant mitochondrial membrane potential.[12, 37-41] Our approach involves chemically modifying the surface of the engineered VLP Qβ using a synthetic linker that separates the TPP from the viral surface once the capsid enters the cytosol. We prepared a dibromomaleimide-triphenylphosphonium (DB-TPP) linker (Fig. 1A-B) via direct EDC coupling. The dibromomaleimide moiety reacts with thiol groups in a two-step reaction,[42] each step having a half-life of seconds.[35, 43] Qβ contains 180 disulfide bonds, each of which can be a potential site for functionalization via this approach. The attachment of DB-TPP to Qβ forms a covalent two-carbon "bridge" between the free thiol groups in reduced Qβ (Fig. 1B).[43, 44] First, Qβ is reduced using tris(2-carboxyethyl) phosphine (TCEP), which is confirmed by electrophoretic mobility in non-reducing 10% sodium dodecyl sulfate-polyacrylamide gel electrophoresis (SDS-PAGE). The starting Qβ pentameric and hexameric subunit bands are shown in Fig. 1C, which are converted almost exclusively into monomer bands following reduction. Ellman's assay further confirms reduction against a cysteine standard curve (Fig. S1), where approximately 95% of the disulfides on Qβ were found to be reduced into free thiols. The bioconjugation was then completed following the addition of the DB-TPP molecule, and within a few minutes, conjugation was confirmed by a significant visible increase in yellow-green fluorescence under UV light. Electrophoretic mobility using non-reducing 10% SDS-PAGE (Fig. 1C) shows the reformation of the hexameric and pentameric subunits and a slight upward migration of these bands compared to unreduced Qβ. These bands are also fluorescent under UV light, providing further evidence for the successful conjugation of the maleimide-TPP (M-TPP) linker to Qβ. Native agarose electrophoresis of the conjugate, visualized by UV and Coomassie staining, shows less migration toward the positive electrode than unfunctionalized Qβ, which is attributed to the additional positive charge from the TPP moiety. Intensity from the newly formed Qβ M-TPP conjugate (Qβ-M-TPP) can be measured by fluorescence spectroscopy at 540 nm (excitation 400 nm) (Fig. 1D).[35] This emergence of yellow fluorescence following the successful displacement of the bromides and formation of the dithiolated conjugate has been attributed to lower self-quenching and a decrease in the frequency of emission-decreasing collisional events with solvent molecules following conjugation.[35, 44] We found no changes in the size of Qβ-M-TPP compared to Qβ as determined by size exclusion chromatography (SEC) and dynamic light scattering (DLS) analyses (Fig. 1E and 1F) – Qβ and Qβ-M-TPP have hydrodynamic radii (R_h) of 31.92 ±10.76 and 31.22 ±10.36 nm respectively. Transmission electron microscopy (TEM) confirms that the morphology of conjugated Qβ-M-TPP is unchanged (Fig. 1G). ζ- potential measurements show an increase in positive charge on Qβ after conjugation, which arises from the cationic nature of TPP (Fig. S2). Lastly, the total number of conjugated linkers per capsid was determined to be approximately 140 linkers (78% of surface disulfide bonds) per Qβ by Ellman's assay (Fig. S1). Glutathione (GSH) tripeptide is the most abundant thiol species in the cytosol of living cells and acts as a biological reducing agent. The intracellular concentration of GSH is (1–10 mM), whereas the concentration
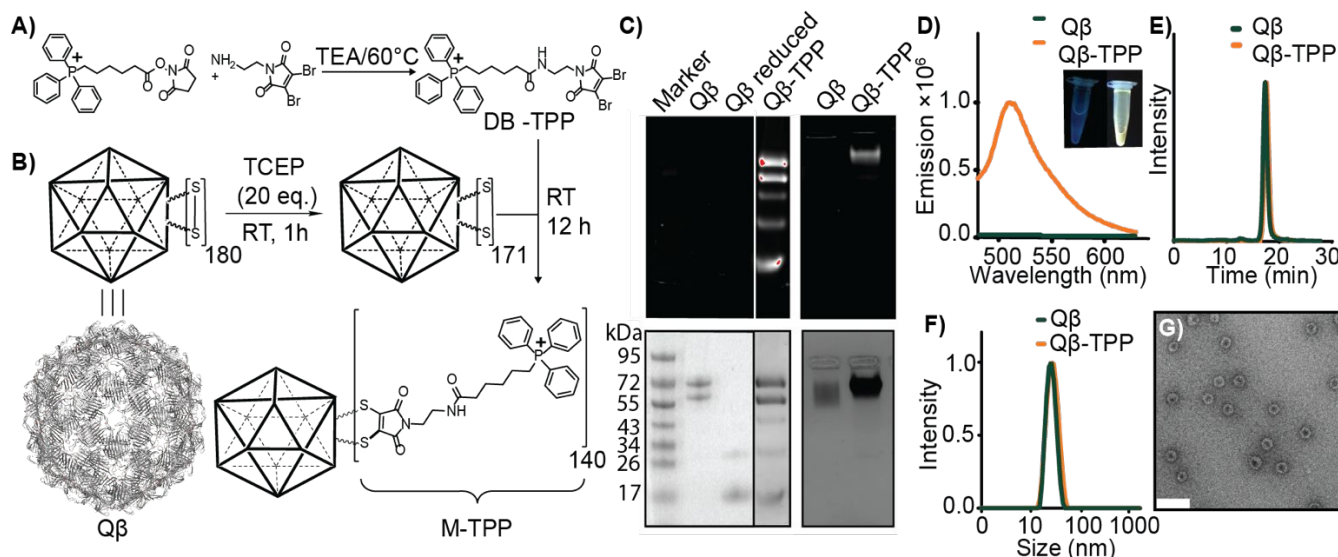
Fig 1. A) Synthesis of dibromomaleimide-TPP (DB-TPP) linker followed by B) bioconjugation strategy on Qβ. C) Electrophoretic mobility analyses of Qβ before and after DB-TPP conjugation using 10% SDS-PAGE (left) and 1% agarose (right) gels showing successful bioconjugation of the maleimide linker to Qβ, forming Qβ-M-TPP. SDS-PAGE shows the successful reduction of the higher-order structures and their reappearance after conjugating DB-TPP. The fluorescence imaging of agarose (top right) shows the maleimide fluorescence at the same spot of the Coomassie-stained band. D) Fluorescence spectra of Qβ-M-TPP and Qβ before and after conjugation with DB-TPP (ex/em 400/540 nm) with a photograph showing the reaction mixtures of Qβ-M-TPP under 365 nm UV lamp illumination. E) SEC of Qβ-M-TPP and Qβ. After bioconjugation, F) DLS and G) TEM of Qβ-M-TPP show no aggregation or structural change. Scale bar = 100nm.

drops to about 1–10 µM in extracellular matrices.[45,46] Therefore, the cytosol of mammalian cells contains 100–1000 times the amount of GSH compared to the extracellular compartment creating a thiol-rich environment. This environment presents a unique opportunity for cargo's specific and selective cytosolic release via a thiol exchange reaction with our disulfide-linker on Qβ. We hypothesized that the Qβ-M-TPP formulation, with its thiol-maleimide bonds, will undergo retro-Michael additions with the abundant GSH, separating most of the TPP from the VLP surface and forming GSH-M-TPP. To verify this supposition, we labeled dibromomaleimide with the small fluorescent molecule FITC (Fig. S3) and did an ex-vitro thiol-exchange experiment by subjecting the Qβ-M-FITC conjugate to conditions that would approximate the cytoplasm (20 mM HEPES, 100 mM KCl, 1 mM MgCl$_2$, 1 mM EDTA, 1 mM glutathione, pH 7.4, 37 °C).[44,47] Scrambling of M-FITC linker from Qβ onto GSH was analyzed using SEC. As expected, data shown in Fig. S4 indicates cleavage of the M-FITC linker from Qβ and attachment to GSH. The starting retention time of Qβ-M-FITC is 16.8 min in the SEC trace. After 24 h, however, we observed the formation of new FITC-labeled oligomers of GSH with lower MW compared to Qβ, having retention times of 21.3 and 27.9 min. We note that there is still Qβ-M-FITC after 24 h, though the peak height decreased about 61% over 24 h. This observation suggests such conjugates have the potential to cleave in the cytosol of cells; however, to determine if the amount of cleavage was sufficient, we moved to *in vitro* experiments.

Results and discussion

Cellular Uptake, Cytotoxicity, and Delivery of Qβ-M-TPP

We next moved to *in vitro* studies of the conjugates. Human lung cancer is one of the fastest-growing malignant tumors, and its treatment is limited by intrinsic resistance to certain anticancer drugs, that exert their therapeutic effect within the cell's cytoplasm. For *in vitro* studies, non-small cell lung cancer (NSCLC) A594 human adenocarcinoma lung cells were employed to evaluate the cell viability, cellular uptake, and cytosolic delivery following treatment with the designed formulation. To visualize the protein trafficking into and throughout the cell, we used fluorescently engineered Qβ that contains Green Fluorescent Protein within the viral capsid—Qβ(GFP).[48] The viability of A549 cells following different treatments with Qβ(GFP) and Qβ(GFP)-M-TPP was measured by 3-(4,5-dimethylthiazol-2-yl)-2,5-diphenyltetrazolium bromide (MTT) assay and compared to that of untreated controls. As shown in Fig. 2A, we found exceptionally low toxicity, even at high concentrations, with cell viabilities more significant than 97% following exposure to each formulation at a 2 mg/ml concentration after a 4 h incubation. These results indicate that the Qβ particles decorated with M-TPP should have high biocompatibility and low toxicity. Next, we treated cells with Qβ(GFP) or Qβ(GFP)-M-TPP and quantified cellular uptake with flow cytometry after fixing the cells. We observed a slight increase in uptake in cells treated with Qβ(GFP)-M-TPP, as compared to Qβ(GFP), which suggests modifying Qβ with the linker does not significantly affect particle uptake (Fig. 2B). We next used fluorescence microscopy to visualize uptake and cytosolic delivery

of Qβ(GFP)-M-TPP in fixed A549 cells. The obtained images revealed that the delivered Qβ(GFP)-M-TPP was evenly distributed as green fluorescence throughout the cytosol (Fig. 2D) while Qβ(GFP) shows punctate fluorescence dots that indicate endosomal entrapment (Fig. 2C). We also tested the cytosolic delivery of Qβ(GFP)-M-TPP vs Qβ(GFP) in live A549 cells as shown in Fig. S5A. In the live-cell imaging studies, we observed the same results as in fixed cells. The Qβ(GFP)-M-TPP green fluorescence was diffuse in the cells, proving the ability of Qβ(GFP)-M-TPP to escape the endosome and reach the cytosol; however, we saw very little green fluorescence in live cells treated with Qβ(GFP) because it was quenched from the acidic environment of the endosome.[32, 48] The live cells were stained with Lysotracker and nuclear stain Hoescht dye, as shown in Fig. S6 and S7. Furthermore, to emphasize that TPP does not deliver Qβ(GFP) to the mitochondria because of cytosolic cleavage, the treated and fixed cells were stained with MitoTracker™ Deep Red FM. As shown in Fig. 2E and 2F, there is no overlap between the red fluorescence of MitoTracker and the green fluorescence of Qβ(GFP).

We then progressed to the *in vivo* evaluation of our Qβ system. To overcome the autofluorescence of lung tissue, which fluoresces in the GFP channel, we used a genetically modified Qβ expressing small Ultra-Red Fluorescent Protein (smURFP), smURFP@Qβ, which we have previously shown to overcome the ambiguities of imaging in highly autofluorescent tissues.[49] smURFP@Qβ-M-TPP was attached using the same methods as our GFP variant (Figure S8) and the fluorescent protein did not seem to influence the bioconjugation chemistry. Mice were administered three doses of 2 mg ml^{-1} smURFP@Qβ or smURFP@Qβ-M-TPP through intratracheal lung lavage. After 6 h, their lungs were collected and processed for confocal microscopy. Without the M-TPP linker, magenta fluorescence from the smURFP@Qβ appears localized within pockets (Fig. 2G) around the cells. We could not determine where the VLP was localized in the lung tissue, but it seemed clear that it was not in the cytosol. However, with the endosome-escaping linker, more overlap of smURFP fluorescence was observed diffusely in the tissue (Fig. 2H), suggesting that delivery of smURFP@Qβ-M-TPP was to the cytosol of the cells. Since the fluorescence is so diffuse throughout the cells, we believe that our linker conjugates allowed for the evasion of endosomal trapping and lysosome degradation of smURFP@Qβ.
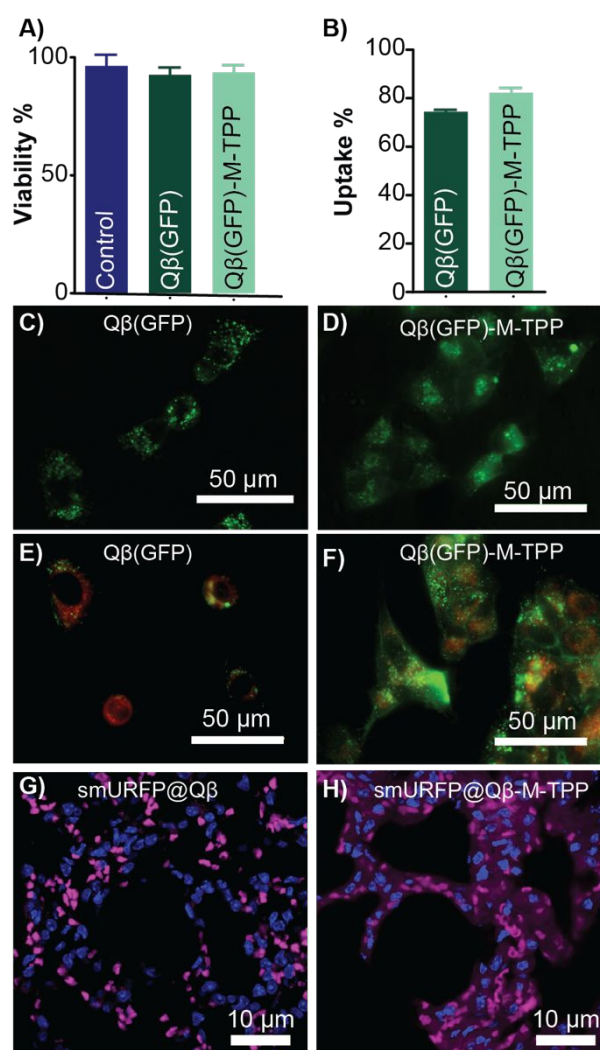

Fig. 2. A) Cell viability of A549 lung cancer cells after treatment with Qβ(GFP) and Qβ(GFP)-M-TPP (2 mg/ml) for 4 h at 37 °C. B) Flow cytometry was used to assess the uptake of Qβ(GFP)-M-TPP and Qβ(GFP) (2 mg/ml) in fixed A549 cells after incubation at 37 °C for 4 h. C) Fluorescence microscopy images of fixed A549 cells treated with Qβ(GFP) showing punctate dots coming from endocytic uptake and A549 cells treated with D) Qβ(GFP)-M-TPP showing diffuse green fluorescence related to the cytosolic release of Qβ(GFP). Color code: green: Qβ(GFP). Scale bar = 50 μm. E) Fluorescence micrograph of Qβ(GFP) and F) Qβ(GFP)-M-TPP in fixed A549 cells stained with MitoTracker showing no mitochondrial colocalization of Qβ(GFP)-M-TPP. Color code: red: MitoTracker Deep Red FM and green: Qβ(GFP). Scale bar = 50 μm. G) Fluorescence microscopy images of *ex vivo* lung cells smURFP@Qβ in endosomal traps, observed by bright localized fluorescence, and H) enhanced delivery of smURFP@Qβ-M-TPP conjugates to the cytosol of cells indicated by diffuse magenta fluorescence. Color code: blue: DAPI and magenta: smURFP@Qβ. Scale bar = 50 μm.

To further prove the role of the intermediate linker in thiol exchange cleavage and cytosolic delivery, we labeled the lysine residues of Qβ with TPP using a non-cleavable linker.[13] We expected that functionalizing the Qβ surface with TPP without a cleavable linkage would traffic our carrier, Qβ, to the mitochondria. To test this, we covalently attached the TPP to the free amine groups on the surface of Qβ through NHS ester chemistry (Fig. 3A).[50]

Curiously, unlike the attachment at the disulfides, this functionalization resulted in a sensitivity of the Qβ towards ions in the buffer and poor colloidal stability and precipitation when preparing the sample in cell media (DMEM) for *in vitro* studies. Efforts to control this by reducing the number of TPP molecules to a relative minimum were only modestly successful. We previously found that attaching lipophilic drug molecules to the Qβ lysines creates problems for colloidal stability. By attaching polyethylene glycol (PEG) linkers across the disulfides, we could significantly increase the solubility and stability of the Qβ.[51] Here, we applied the same strategy and first decorated Qβ with dibromomaleimide-PEG at the reduced disulfide bonds, followed by the attachment of TPP moieties to the free lysines. Bioconjugation conditions were optimized, and particle size, surface charge, and morphology before and after conjugation were characterized, as shown in Fig. 3B-D. The mitochondria-targeting of Qβ-M-TPP was assessed *in vitro* on another common drug-resistant non-small cell lung cancer cell model H2073 by confocal fluorescence microscopy. Cells treated with Qβ(GFP)-M-TPP and stained with MitoTracker Deep Red FM were used to determine the colocalization of the green fluorescence of Qβ(GFP) conjugates with the mitochondria (Fig. 3E). Colocalization was calculated using Pearson's coefficient (ρ) and NIH ImageJ. From the results, the targeted conjugates show greater colocalization with MitoTracker (ρ = 0.56) than the non-targeted conjugates (ρ = 0.28), suggesting modest colocalization within the mitochondria. Notably, a significant number of particles were still observed in the endosome/lysosome (punctate dots), but there was no diffuse fluorescence indicative of cytosolic delivery.
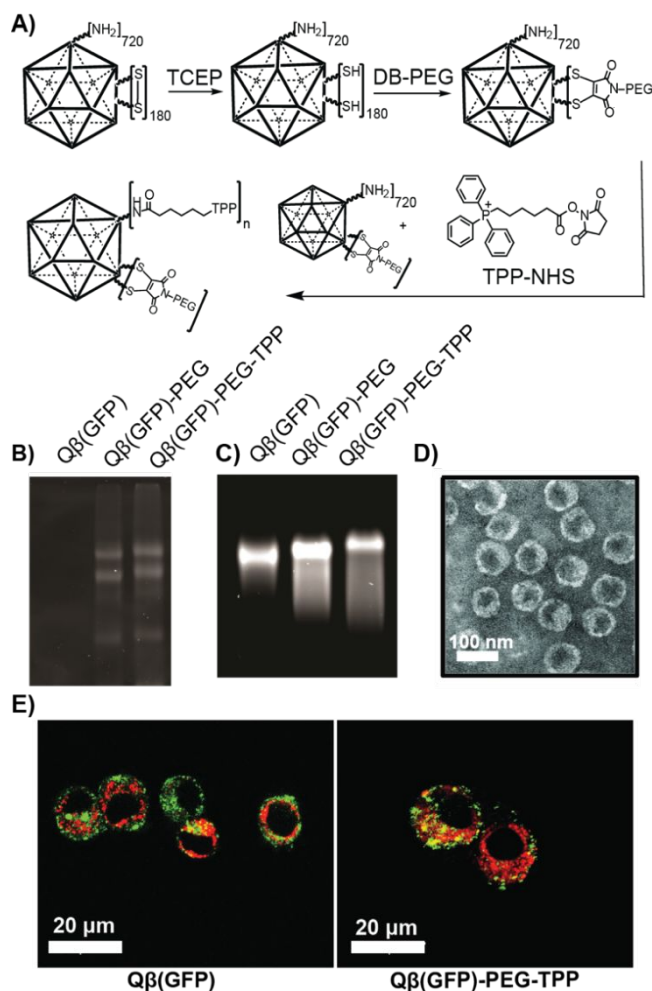

Fig. 3. A) Conjugation scheme of Qβ-PEG-TPP. Qβ first is reduced with TCEP, followed by adding Dibromomaleimide-PEG (DB-PEG). Conjugation of TPP-NHS with surface amines is then performed using TPP-NHS. Characterization of Qβ-PEG-TPP conjugation B) 10% SDS gel C) 1% agarose gel D) TEM (scale bar: 100 nm). E) Fluorescence micrographs of NSCLC H2073 cells treated with Qβ(GFP) and Qβ(GFP)-PEG-TPP. Qβ(GFP)-PEG-TPP is driven into the mitochondria with greater colocalization efficiency (ρ), which is calculated using Pearson's coefficient, colocalization (ρ = 0.56) compared to non-targeted conjugates (ρ = 0.28). Color code: green: Qβ(GFP), red: MitoTracker Deep Red FM.

Delivery of siRNA to Efficiently Silence Luciferase *in vitro*

Proving delivery into the cytosol using optical microscopy can be ambiguous. Thus, to further verify cytosolic entry and check the applicability of our delivery system, we used Qβ-M-TPP to deliver luciferase-targeted siRNA (siLuc), an siRNA (small-interfering RNA) probe capable of silencing luciferase expression in HeLa luciferase cells.[52] This work aims to demonstrate the cytosolic delivery of a VLP; proving its capability to enhance siRNA delivery compared to existing transfection agents is beyond the scope of this paper. With that said, siRNA is not only a useful *in vitro* tool, it is also a powerful therapeutic tool that inhibits specific messenger RNA (mRNA) expression in the cytosol and effectively downregulates

the gene expression processes.[53] However, siRNA is highly anionic, has a relatively large molecular weight, and quickly degrades in cell media. Naked siRNA cannot readily penetrate cell membranes and reach the cytoplasm; therefore, we hypothesized that encapsulation of siRNA in Qβ-M-TPP could enhance cytosolic delivery and improve gene silencing compared to free siRNA or Qβ that lacked cleavable TPP groups.

Qβ capsid formation occurs in the recombinant E. coli expression system through charge-mediated interactions between the negatively charged random E. coli RNA and positively charged Qβ CP subunits.[34, 54] Disulfide formation in the biological synthesis of Qβ occurs after the capsid has self-assembled, likely following exposure to molecular oxygen in the bacteria or following cell lysis. Given the highly negative charge of siRNA,[55] we hypothesized siLuc could promote assembly of Qβ capsids and addition of the DB-TPP could "sew" the capsid up in a one-pot process. Specifically, we anticipated that we could reduce the Qβ with 1,4-dithioerithrol (DTT) and disassemble the capsid in a salt solution. The addition of siLuc could then promote capsid reassembly, and DB-TPP could seal the capsid *in situ* as the last step (Fig. 4A).
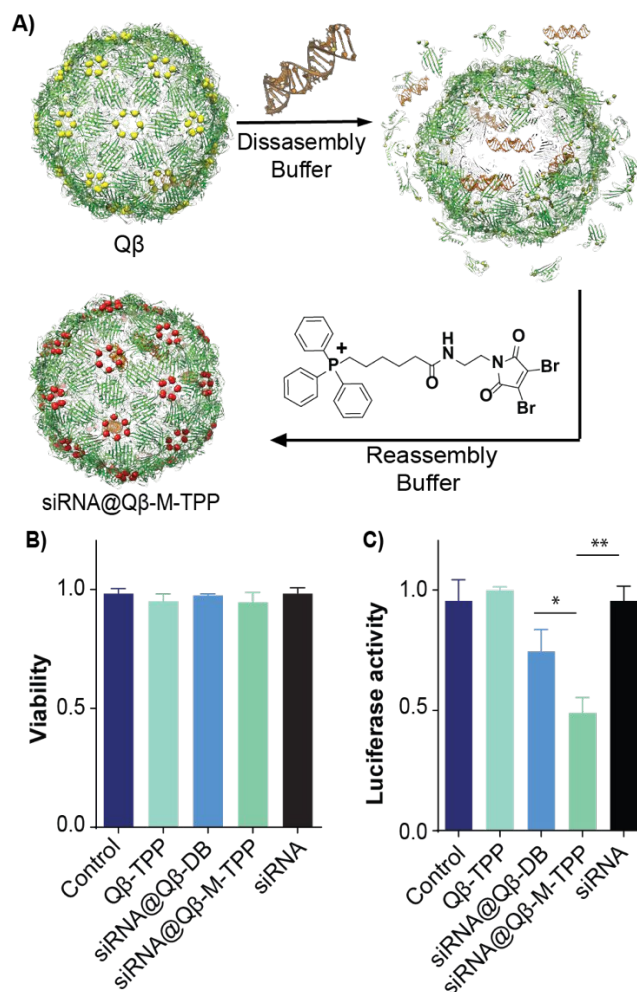

Fig. 4. A) Scheme for disassembly of Qβ virions to CPs, then the reassembly around siRNAs to make siRNA@Qβ-M-TPP. B) Cell viability and relative levels of luciferase expression in HeLa luciferase cells after various treatments.

First, purified Qβ VLPs were disassembled into CPs through a salt-controlled disassembly method[16, 32] by adding the reducing agent DTT and magnesium chloride (MgCl₂), which facilitates the recovery and precipitation of packed RNA. Next, the obtained CP was purified using dialysis and centrifugation. SEC, 1% agarose, and 10% SDS gel electrophoresis were used to verify the E. Coli RNA was removed and the Qβ disassembled into CPs (Fig. S9). Data show the presence of CPs through a single band in SDS-PAGE and positive charge migration through agarose gel electrophoresis with a change in capsid retention time by SEC. Reassembly proceeded in the presence of siRNA under DTT-reducing conditions. We found that a siRNA to CP ratio of 1:4 was sufficient to promote complete capsid formation.

Finally, we proceeded with the surface installation of TPP directly in the reassembly buffer by adding 50 eq of DB-TPP to the solution. Absorbance at A260/280 ratio was used to confirm complete siLuc packing. We were happy to find that the A260/280 ratio increased from 0.87 (pre-siLuc packing) to 2.0 (post-siLuc packing). Direct

observation of the VLP assemblies was done by TEM. Fig. S10 shows well-formed VLPs after the encapsidation of the siRNA, which is further confirmed by 1% agarose and 10% SDS gel electrophoresis showing the hex ametric and pentameric subunits of siRNA@Qβ-M-TPP exhibiting similar integrity to native Qβ (Fig. S10). To assess the *in vitro* cytosolic delivery of siRNA using siRNA@Qβ-M-TPP, we compared the silencing ability of naked siRNA, siRNA loaded in Qβ without the M-TPP linker, and siRNA loaded in Qβ-M-TPP in luciferase-expressing HeLa cells. The cell viability and luciferase expression were measured using standard One-Glo Tox luciferase and cell viability assay. It was found that after 24 h, all treatment groups had high cell viability (Fig. 4B), but the siRNA@Qβ-M-TPP treated cells showed a significantly lower luciferase expression (47%) as compared to free siRNA treated cells (93%) (Fig. 4C). Considering that uptake of Qβ and Qβ-M-TPP are comparable, this result further proves the cytosolic delivery of our formulation and demonstrates — as a proof-of-principle — that we can enhance cytosolic siRNA delivery via this approach.

Conclusions

Most nanoparticle-based delivery systems must escape the endosome and lysosome to reach the cytosol for efficient therapeutic and diagnostic action. In this work, we chemically modify the surface of an engineered protein model, Qβ, using a glutathione-sensitive linker attached to a lipophilic cation to overcome endosomal entrapment and achieve cytosolic delivery. Our approach using a ''sheddable linker'' was further confirmed when we observed no cytosolic delivery without a GSH cleavable linker. As proof-of-principle, we successfully demonstrate the applicability of our synthetic bioconjugation strategy in the cytosolic delivery of a VLP-carrying GFP *in vitro,* smURFP *in vivo*, and siRNA *in vitro*. Ultimately, both *in vitro* and *in vivo* studies have the potential to be useful for therapeutic and clinical applications and will be considered for future work.

Author Contributions

JJG conceived the project and wrote the manuscript with AS and LH. AS, LH, NA, AT, and HF synthesized all compounds. AS, AB, LH, and NA performed bioconjugation and characterization AS, LH, OB, and NA conducted *in vitro* experiments and fluorescence microscopic imaging. LH, FC, and IT performed *in vivo* experiments, and IT and SC conducted confocal imaging. ZC performed PEGTPP conjugation and *in vitro experiments*. AS and FC conducted RNA encapsulation and characterization. NA duplicated the synthesis and *in vitro* work to demonstrate rigor.

Conflicts of interest

There are no conflicts to declare.

Acknowledgments

Notes and references

1   V. Sharma and V. Kalyani, *International Conference on Information, Communication, Instrumentation and Control (ICICIC)*, 2017, 1-5.

2   P. J. McMillan, T. J. Strovas, M. Baum, B. K. Mitchell, R. J. Eck, N. Hendricks, J. M. Wheeler, C. S. Latimer, C. D. Keene and B. C. Kraemer, *Acta Neuropathol Commun*, 2021, **9**, 117.

3   Y. Z. Lin Hou, Xuemei Yang, Chunyu Tian, Yingshan Yan, and J. S. Hongling Zhang, Huijuan Zhang and Zhenzhong Zhang, *ACS Appl. Mater. Interfaces*, 2019, **11**, 225-268.

4   Qian Cao, Hang Zhang, Liang Hao, Gang-Gang Yang, Liang-Nian Ji and Zong-Wan Mao, *Chem. Commun*, 2019, **55**, 7852-7855.

5   V. Oorschot, Katrien Remaut, Kevin Braeckmans, Judith Klumperman, Stefaan C. De Smedt,, *Journal of Controlled Release*, 2014, **195**, 29-36.

6   William B. Liechty, Rebekah L. Scheuerle, Julia E. Vela Ramirez, Nicholas A. Peppas,, *International Journal of Pharmaceutics*, 2019, **562**, 249-257.

7   S. Antimisiaris, S Mourtas, K Papadia, *International Journal of Pharmaceutics*, 2017, **525**, 293-312.

8   J. C. Kim D, Kim JH, Kim MS, Yoon CH, Choi IS, Kim SH, Bae YS., *Exp Cell Res.* , 2009, **312**, 1277-1288.

9   M. Uchida, B. Maier, H. K. Waghwani, E. Selivanovitch, S. L. Pay, J. Avera, E. Yun, R. M. Sandoval, B. A. Molitoris, A. Zollman, T. Douglas, T. Hato. *J Clin Invest*. 2019, **129**, 3941-3951.

10   W. Jiang, H. Zhang, J. Wu, G. Zhai, Z. Li, Y. Luan, S. Garg, *ACS Appl. Mater. Interfaces*, 2018, **10**, 34513-34523.

11   L. F. Yousif, K. M. Stewart and S. O. Kelley, *Chembiochem*, 2009, **10**, 1939-1950.

12   G. I. Kaupova. Lucia Ya. Zakharova, Dinar R. Gabdrakhmanov, Gulnara A. Gaynanova, Elena A. Ermakova, Alexander R. Mukhitov, Irina V. Galkina,   Sergey V. Cheresiz, Andrey G. Pokrovsky, Polina V. Skvortsova, Yuri V. Gogolevc and Yuriy F. Zuev *Phys. Chem. Chem Phys.*, 2019, **21**, 16706-16717.

13   J. Zielonka, J. Joseph, A. Sikora, M. Hardy, O. Ouari, J. Vasquez-Vivar, G. Cheng, M. Lopez and B. Kalyanaraman, *Chem Rev*, 2017, **117**, 10043-10120.

14   Gantumur Battogtokh, Yeon SuChoia, Dong Seop Kang, Sang Jun Park, Min Suk Shim, Kang Moo Huh, Yong-Yeon Cho, Joo Young Lee, Hye Suk Lee, Han Chang Kang, *Acta Pharmaceutica Sinica B*, 2018, **8**, 862-880.

15   M. P. Murphy, *Biochimica et Biophysica Acta (BBA)-Bioenergetics*, 2008, **1777**, 1028-1031.

16   A.C. Gomes, E. S. Roesti, A. El-Turabi and M. F. Bachmann, *Vaccines (Basel)*, 2019, **7**, 47.

17   A. M. Wena and N. F. Steinmetz, *Chem. Soc. Rev.*, 2016, **45**, 4074.

18   N. F. Steinmetz, *Nanomedicine: Nanotechnology, Biology and Medicine*, 2010, **6**, 634-641.

19   Oliver Ast, Andrezj Citkowicz, Linda Cashion, Brent Larsen, Gabor M. Rubanyi, Richard N. Harkins, Harald Petry, *Molecular Therapy*, 2005, **11**, S68.

20   P. Parsamian, Y. Liu, C. Xie, Z. Chen, P. Kang, Y. H. Wijesundara, N. M. Al-Kharji, R. N. Ehrman, O. Trashi, J. Randrianalisoa, X. Zhu, M. D'Souza, L. A. Wilson, M. J. Kim, Z. Qin and J. J. Gassensmith, *ACS Nano*, 2023, DOI: 10.1021/acsnano.3c00638.

21   A. Shahrivarkevishahi, L. M. Hagge, O. R. Brohlin, S. Kumari, R. Ehrman, C. Benjamin and J. J. Gassensmith, *Materials Today Chemistry*, 2022, **24**, 100808.

22   M. Dharmarwardana, A. F. Martins, Z. Chen, P. M. Palacios, C. M. Nowak, R. P. Welch, S. Li, M. A. Luzuriaga, L. Bleris, B. S. Pierce, A.

D. Sherry and J. J. Gassensmith, *Molecular Pharmaceutics*, 2018, **15**, 2973-2983.

23   N. L. Zhuo Chen, Luxi Chen, Jiyong Lee, Jeremiah J. Gassensmith, *Small*, 2016, **12**, 4563-4571.

24   Wu W, Hsiao, SC, Carrico ZM, Francis MB., *Angew Chem Int Ed Engl.*, 2009, **48**, 9493-9497.

25   Pawel Kraj, Ekaterina Selivanovitch, Byeongdu Lee, and Trevor Douglas, *Biomacromolecules*, 2021, **22**, 2107-2118.

26   C. E. Benjamin, Z. Chen, P. Kang, B. A. Wilson, N. Li, S. O. Nielsen, Z. Qin and J. J. Gassensmith, *J Am Chem Soc*, 2018, **140**, 17226-17233.

27   Arezoo Shahrivarkevishahi, Michael A. Luzuriaga, Fabian C. Herbert, Alisia C. Tumac, Olivia R. Brohlin, Yalini H. Wijesundara, Abhinav V. Adlooru, Candace Benjamin, Hamilton Lee, Perouza Parsamian, Jashkaran Gadhvi, Nicole J. De Nisco, and Jeremiah J. Gassensmith, *J. Am. Chem. Soc.*, 2021, **143**, 16428-16438

28   Minseok Kwak, Inge J. Minten, Diana-Milena Anaya, Andrew J. Musser, Melanie Brasch, Roeland J. M. Nolte, Klaus Müllen, Jeroen J. L. M. Cornelissen, and Andreas Herrmann, *J. Am. Chem. Soc.,* 2010, **132,** 7834–7835

29   Candace Benjamin, Olivia Brohlin, Arezoo Shahrivarkevishahi, Jeremiah J. Gassensmith, Elsevier, 2020, 153-174,

30   Steven D. Brown, Jason D. Fiedler and M. G. Finn, *Biochemistry*, 2009, **48**, 11155–11157.

31   Olivia Brohlin, Candace Benjamin, Arezoo Shahrivarkevishahi, Jeremiah J. Gassensmith*, Elsevier,* 2020, 153-174.

32   Zhuo Chen, Candace E. Benjamin, Olivia R. Brohlin, Hamilton Lee, Arezoo Shahrivarkevishahi, Stefanie Boyd, Duane D. Winkler and Jeremiah J. Gassensmith, *Nanoscale*, 2020, **12**, 9124-9132.

33   Duane E. Prasuhn Jr., Patrik Singh Erica Strable, Steven Brown, Marianne Manchester, and M. G. Finn, *J. Am. Chem. Soc.*, 2008, **130**, 1328–1334.

34   Fabian C. Herbert, Olivia R. Brohlin, Tyler Galbraith, Candace Benjamin, Cesar A. Reyes, Michael A. Luzuriaga, Arezoo Shahrivarkevishahi, and Jeremiah J. Gassensmith, *Bioconjugate Chem.*, 2020, **31**, 1529-1536.

35   Zhuo Chen, Stefanie D. Boyd, Jenifer S. Calvo, Kyle W. Murray, Galo L. Mejia, Candace E. Benjamin, Raymond P. Welch, Duane D. Winkler, Gabriele Meloni, Sheena D'Arcy, and Jeremiah J. Gassensmith, *Bioconjugate Chem*, 2017, **28**, 2277–2283.

36   Bingjie Hao, Wei Li, Sen Zhang, Ying Zhu, Yongjun Li, Aishun Dinga and Xiaoyu Huang *Polym. Chem.*, 2020, **11**, 2194-2204.

37   Guoyao Wu, Yun-Zhong Fang, Sheng Yang, Joanne R. Lupton, Nancy D. Turner, *The Journal of Nutrition*, 2004, **134**, 489–492.

38   Y. H. Wijesundara, F. C. Herbert, S. Kumari, T. Howlett, S. Koirala, O. Trashi, I. Trashi, N. M. Al-Kharji and J. J. Gassensmith, *Virology*, 2022, **577**, 105-123.

39   M. F. Ross, G. F. Kelso, F. H. Blaikie, A. M. James, H. M. Cochemé,A. Filipovska, T. Da Ros, T. R. Hurd, R. A. J. Smith, and M. P. Murphy, *Biochemistry (Moscow)*, 2005, **70**, 222-230.

40   T. K. Lin, G. Hughes, A. Muratovska, F. H. Blaikie, P. S. Brookes, V. Darley-Usmar, R. A. Smith and M. P. Murphy, *J Biol Chem*, 2002, **277**, 17048-17056.

41   Lee M. Booty, Justyna M. Gawel, Filip Cvetko, Thomas Krieg, Richard C. Hartley, Michael P. Murphy, *Cell Chemical Biology*, 2019, **26**, 449-461.

42   A. Wall, A. G. Wills, N. Forte, C. Bahou, L. Bonin, K. Nicholls, M. T. Ma, V. Chudasama and J. R. Baker, *Chem Sci*, 2020, **11**, 11455-11460.

43   Arianna Gennaria, Jennifer Wedgewood, Enrique Lallana, Nora Francini, NicolaTirelliab, *Tetrahedron*, 2020, **76**, 131637.

44   Montserrat Marí, Estafania de Gregorio, Cristina de Dios, Vicente Roca-Agujetas, Blanca Cucarull , Anna Tutusaus, Albert Morales and Anna Colell, *Antioxidants*, 2020, **9**, 909.

45   Mathew P. Robin, Paul Wilson, Anne B. Mabire, Jenny K. Kiviaho, Jeffery E. Raymond, David M. Haddleton, and Rachel K. O'Reilly, *J. Am. Chem. Soc.*, 2013, **135**, 2875-2878.

46   G. M. Enns and T. M. Cowan, *J. Clin. Med.*, 2017, **6**, 50.

47   M. C. Yi and C. Khosla, *Annu Rev Chem Biomol Eng*, 2016, **7**, 197-222.

48   Mark E. B. Smith, Felix F. Schumacher, Chris P. Ryan, Lauren M. Tedaldi, Danai Papaioannou, Gabriel Waksman, Stephen Caddick, and James R. Baker, *J. Am. Chem. Soc.*, 2010, **132**, 1960-1965.

49   I.Trashi, M. Z. Durbacz, O. Trashi, Y. H. Wijesundara, R. H. Ehrman, A. C. Chiev, C. B. Darwin, F. C. Herbert, J. Gadhvi, N. J. De Nisco, S. O. Nielsen, J. J. Gassensmith, *J. Mater. Chem. B*, 2023, **11**, 4445-4452

50   M. H. Jin-Kyu Rhee, Jason D. Fiedler, Steven D. Brown, Florian Manzenrieder, Hiroaki Kitagishi, Corwin Nycholat, James C. Paulson, and M.G. Finn, *Biomacromolecules*, 2011, **12**, 3977-3981.

51   F. J. Kneen M, Li Y, Verkman AS., *Biophys J.* , 1998, **74**, 1591-1599.

52   Zhuo Chen, Na Li, Luxi Chen, Jiyong Lee, Jeremiah J. Gassensmith, *Small*, 2016, **12**, 4563-4571.

53   Hong Chang, Jia Lv, Hui Wang, and Yiyun Cheng, *Biomacromolecules*, 2017, **18**, 2371-2378.

54   Alessandro Laganà, Dario Veneziano, Francesco Russo, Alfredo Pulvirenti, Rosalba Giugno, Carlo Maria Croce and Alfredo Ferro, *RNA Bioinformatics*, 2015, **1269**, 393-412.

55   Stacy L. Capehart, Michael P. Coyle, Jeff E. Glasgow, and Matthew B. Francis, *J. Am. Chem. Soc.*, 2013, **135**, 3011-3016.

ARTICLE